2025年臺灣國際科學展覽會 優勝作品專輯

作品編號 160034

參展科別 物理與天文學

作品名稱 Efficient Modelling of Aeroacoustic

Phenomena in Seebeck Sirens: A

Simplified Approach for Real-World

Applications

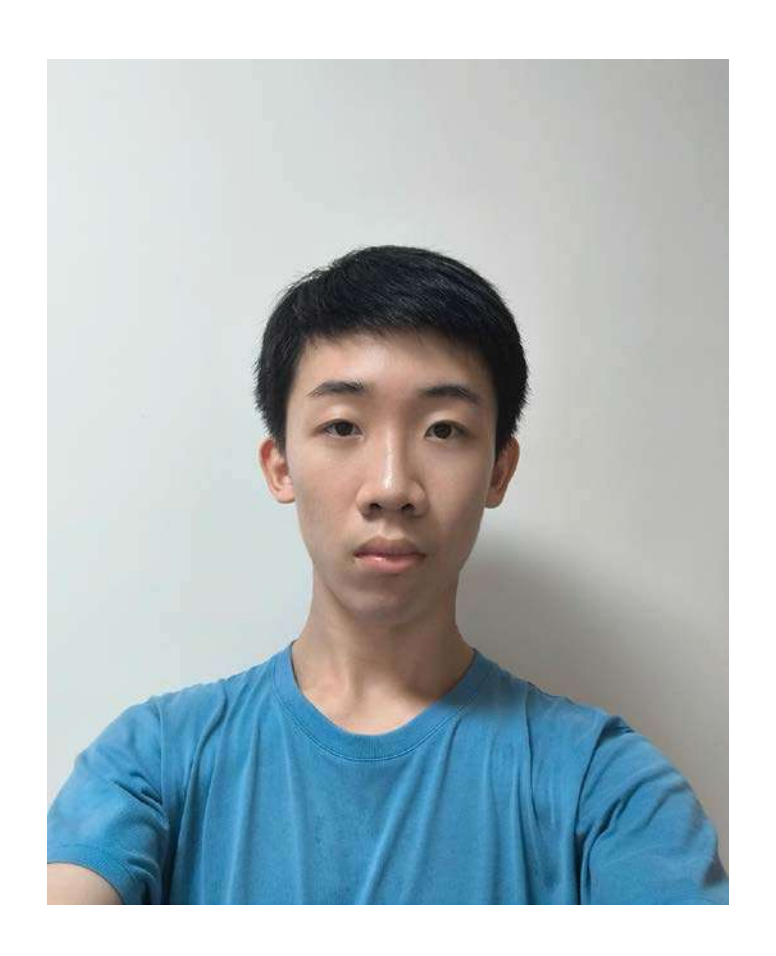
得獎獎項 成就證書

就讀學校 Raffles Institution

指導教師 Se Kuan Pin

作者姓名 Ong Jiunn Xiang

作者照片



Efficient Modelling of Aeroacoustic Phenomena in Seebeck Sirens: A Simplified Approach for Real-World Applications

November 1, 2024

Abstract

This paper presents a simplified but mostly accurate model for the acoustic mechanism of Seebeck sirens. We investigate the impact of key parameters, including the number and size of holes, as well as the angular speed of the disk, on the characteristics of the produced sound. The disk is fabricated using fused deposition modelling 3D printing, and we used a brushless motor, an air compressor, and a shotgun microphone to capture the generated sound. An order of magnitude analysis was conducted on the Navier-Stokes equation to formulate a simplified version. These simplifications allowed for a low computational intensity model relating volume flow rate to sound pressure level, which is used to predict the waveform of sound produced. Our findings reveal that the fundamental frequency of the sound can be precisely predicted by only the rotational frequency of the disk and the number of holes, a relationship validated experimentally. Notably, observed asymmetry in the waveform was attributed to skin drag effects, and this hypothesis was experimentally verified. Our model computes a solution in less than half a second on average: far less than the 21h 47min needed for a $k-\omega$ turbulent model to compute the same phenomenon. The research presents and verifies a simplified model of acoustic mechanics for the sound generated by rotating systems that require little computational resources, which can prove useful in situations where absolute precision is not required, in exchange for ease of computation. For more precise systems, this model serves as a foundation for quickly generating an initial design, paving the way for subsequent iterations using more comprehensive models. The developed model not only serves as a foundation for efficient preliminary designs but also contributes valuable insights into the intersection of fluid dynamics and sound production.

Contents

1	Introduction			3
	1.1	Existing Methods for Aeroacoustics		
	1.2			3
	1.3	Purpo	se	4
2	Mathematical Model			4
	2.1	Pitch of a Seebeck Siren		
	2.2	Waveform of a Seebeck Siren		
		2.2.1	Radially Symmetric Navier Stokes	5
		2.2.2	Order Of Magnitude Analysis	7
		2.2.3	Directional Microphone	11
		2.2.4	Volume flow rate through a Seebeck Siren	12
	2.3	Exper	imental Verification	14
		2.3.1	Experimental Setup	14
		2.3.2	Data Processing Techniques	15
		2.3.3	Experiment Theory Comparison	18
		2.3.4	Observed Asymmetry	20
3	Con	onclusion 23		
4	Fut	Future Work		
A	Derivation of radially symmetric Navier-Stokes in spherical			
	coordinates			
В	Frequency response of microphone			28
\mathbf{C}	Fourier Transform, 4 holes of 1cm radius			28
D	Fourier Transform, 2 holes of 1cm radius			29
${f E}$	Fourier Transform, 4 holes of 0.5cm radius			29

1 Introduction

Sirens are commonly used as sources of loud sound, often used to alert large numbers of people, but there is little research on the timbre of the sound produced. Accurate calculation of acoustic phenomena due to fluid flow has always required intricate and complicated algorithms, often involving the computation of the Navier-Stokes equation. While such techniques can accurately determine the acoustic effects of fluid flow, they are incredibly computationally intensive to solve. They can take many hours to solve a moderately complicated problem, even with significant computational resources. The primary objective of this research is to develop a model with significantly reduced computational complexity compared to existing models, while still being mostly accurate.

1.1 Existing Methods for Aeroacoustics

Aeroacoustics, which is the field investigating the generation and propagation of acoustic phenomena arising from the flow of fluids, often relies on near-complete models of fluids, such as through simplified variants of the Navier-Stokes equations. Despite the existence of many simplified models, the Navier-Stokes equations are still notoriously difficult to solve and require access to powerful computers. For more specific phenomena such as the sound produced by a siren disk, it is possible to simplify the model much further, at the expense of its applicability across diverse fields.

1.2 Background Research

According to Milne (1921), the waveform of a Seebeck Siren is said to be approximated by modelling the siren as a point source with flux proportional to the area of orifice exposed by the holes in the disk [8]. This research,

however, has many limitations. The assumptions made are only qualitatively justified and not experimentally or theoretically verified, and the presented theory assumes that the nozzle and hole are circular and identical.

1.3 Purpose

Due to the lack of research in this area, this paper's objective is to develop a more comprehensive model for Seebeck Siren than existing models, while maintaining the low computation requirements and not resorting to complete numerical models. Although we only investigate Seebeck Sirens in this paper, we aim for the model to be easily adaptable to similar phenomenons and situations.

2 Mathematical Model

2.1 Pitch of a Seebeck Siren

Firstly, we consider the most fundamental aspect of the sound produced by the siren, which is the pitch. The pitch refers to the fundamental frequency, also known as the 1st harmonic, and is the lowest frequency component produced by the siren. Most of the sound produced by the siren exists as multiples of the fundamental, and they represent the periodic component of the sound. We theorize that the fundamental frequency is equal to the frequency at which the holes on the disk are exposed to the air jet. This is because the flux of air through the disk varies at the same frequency at which the holes are exposed to the air jet. This can be represented as:

$$f = q \frac{\omega}{2\pi} \tag{1}$$

Where:

f: is the fundamental frequency of the sound

 ω : is the rotational velocity of the disk

q: is the number of holes on the disk

We attempt to verify this experimentally by measuring the speed of the disk with a tachometer and recording the sound produced. Using Equation 1, we plot the predicted pitch against the rotational frequency of the disk along with our experimentally determined pitch.

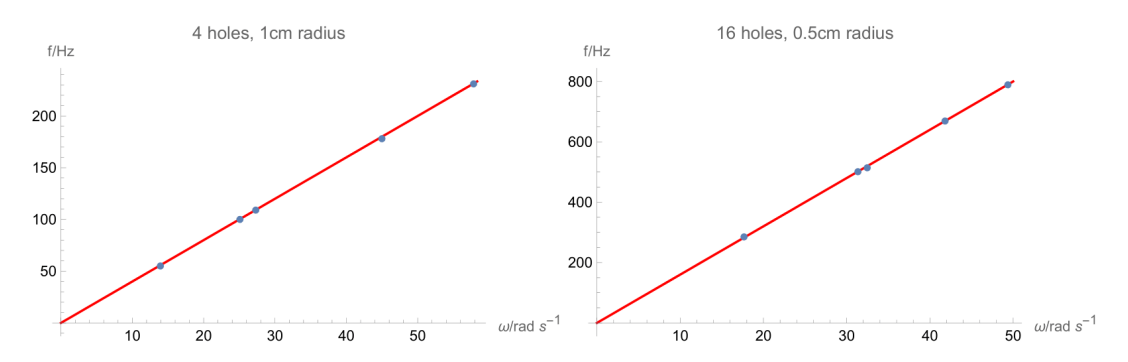


Figure 1: Fundamental frequency against rotational speed for a disk with 16 holes and 4 holes respectively. The red line is theory and the blue dots are experimentally measured.

We observe that there is a near-perfect fit for both disks, which tells us that the fundamental frequency can be consistently predicted using this method.

2.2 Waveform of a Seebeck Siren

2.2.1 Radially Symmetric Navier Stokes

Accurately predicting the waveform produced by a Seebeck Siren comes with great difficulty and would require a numerical simulation of some form of the Navier-Stokes equations. To circumvent this, we can do an order-ofmagnitude analysis of the terms in the Navier-Stokes equations to remove the more difficult-to-solve terms by first converting the Navier-Stokes into spherical coordinates. We begin with the well-known compressible Navier-Stokes equation, which is this:

$$\rho \left(\frac{\partial \mathbf{u}}{\partial t} + (\mathbf{u} \cdot \nabla) \mathbf{u} \right) = -\nabla p + \mu \nabla^2 \mathbf{u} + \frac{1}{3} \mu \nabla (\nabla \cdot \mathbf{u})$$
 (2)

We assume radial symmetry and derive the Navier-Stokes equation in spherical coordinates. The full derivation can be seen in Appendix A, and the result is:

$$\rho\left(\frac{\partial u}{\partial t} + u\frac{\partial u}{\partial r}\right) = -\frac{\partial p}{\partial r} - \frac{8\mu}{3r^2}u + \frac{2\mu}{r}\frac{\partial u}{\partial r} + \frac{4\mu}{3}\frac{\partial^2 u}{\partial r^2}$$
(3)

In this equation, we have partial derivatives of velocity in terms of time and radius. To simplify the equation further, we will now be solving to replace the partial derivatives of velocity with respect to radius with time derivatives. To do this, we begin with the 1D wave equation:

$$\frac{\partial^2 u}{\partial t^2} = c^2 \frac{\partial^2 u}{\partial r^2} \tag{4}$$

$$v(r,t) = v_0 \sin(\omega t + kr) \tag{5}$$

Here, Equation 4 is the 1D wave equation, and Equation 5 is the known solution to Equation 4. k is the angular wavenumber, which is the spatial frequency of a wave, where $k=\frac{\omega}{c}$, and c is the speed of sound. We differentiate the solution with respect to t and r, giving us the following equations:

$$\frac{\partial u}{\partial t} = u_0 \omega \cos(\omega t + kr) \tag{6}$$

$$\frac{\partial u}{\partial r} = u_0 k \cos(\omega t + kr) \tag{7}$$

Using Equation 6 and Equation 7, as well as the definition of the angular wavenumber k, we can express the spatial derivatives in terms of the time derivatives:

$$\frac{\partial u}{\partial r} = \frac{1}{c} \frac{\partial u}{\partial t} \tag{8}$$

$$\frac{\partial^2 u}{\partial r^2} = \frac{1}{c^2} \frac{\partial^2 u}{\partial t^2} \tag{9}$$

We can then use Equation 8 and Equation 9 to replace all the spatial derivatives of velocity with time derivatives in Equation 3, giving us the final form of our Navier-Stokes equation, which assumes radial symmetry and is in spherical coordinates:

$$\rho \frac{\partial u}{\partial t} + \frac{u\rho}{c} \frac{\partial u}{\partial t} = -\frac{\partial p}{\partial r} - \frac{8\mu}{3r^2} u + \frac{2\mu}{cr} \frac{\partial u}{\partial t} + \frac{4\mu}{3c^2} \frac{\partial^2 u}{\partial t^2}$$
(10)

2.2.2 Order Of Magnitude Analysis

Now that we have the final form of our Navier-Stokes equation, we will calculate the order of magnitude estimates for each term to remove any term that is much smaller than the other terms. We begin with the well-known sound amplitude equation:

$$A = 10\log\left(\frac{I}{I_0}\right) \tag{11}$$

Where:

A: is the amplitude of the sound in decibels

I: is the intensity of the sound

 I_0 : is reference intensity of sound, which is $10^{-12}Wm^{-2}$

According to (Urone & Hinrichs, 2020), the intensity of sound and root mean squared particle velocity of sound are related by the following equations [9]:

$$I = \frac{P_{rms}^2}{2\rho c} \tag{12}$$

$$u_{rms} = \frac{P_{rms}}{\rho c} \tag{13}$$

Where:

 P_{rms} : is the root mean squared pressure

 u_{rms} : is the root mean squared particle velocity of air

 ρ : is the density of air

c: is the speed of sound

Combining Equations 11,12,13, we can formulate an equation that describes in u_{rms} in terms of sound amplitude in decibels:

$$u_{rms} = \frac{I_0 10^{\left(\frac{A}{10}\right)}}{\sqrt{\rho c}} \tag{14}$$

We then substitute in the known orders of magnitudes of the constants in the equation to get an estimate for the order of magnitude of u_{rms}

$$A\approx 10^2 dB$$

$$\rho\approx 10^0 kgm^{-3}$$

$$c \approx 10^2 ms^{-1}$$

$$I_0 \approx 10^{-12} Wm^{-2}$$

$$u_{rms} \approx \frac{10^{-12} 10^{\left(\frac{10^2}{10}\right)}}{\sqrt{10^0 10^2}} \approx 10^{-3}$$

From this, we can see that:

$$u \approx 10^{-3} ms^{-1} \tag{15}$$

We also need to estimate the order of magnitude of $\frac{\partial u}{\partial t}$ and $\frac{\partial^2 u}{\partial t^2}$, and to do so, we draw a line from the peak to the trough of the velocity time graph and estimate the gradient of the line:

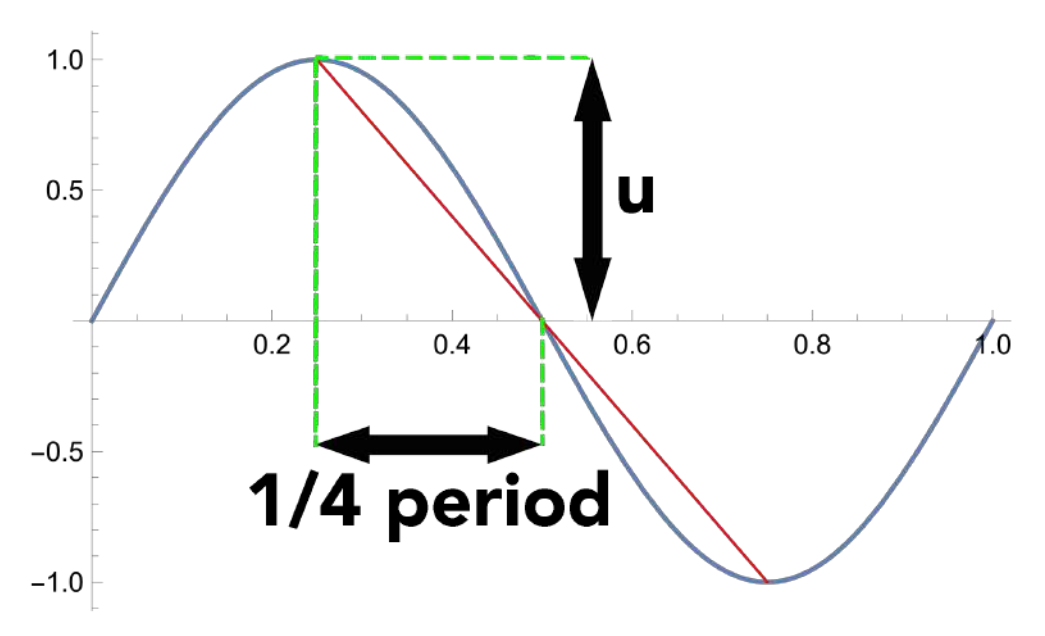


Figure 2: The blue line represents the velocity time graph and the gradient of the red line is the value we use as our $\frac{\partial u}{\partial t}$

To get the gradient of the red line and thus the value of $\frac{\partial u}{\partial t}$, we use the following formula:

$$\frac{\partial u}{\partial t} \approx \frac{u}{\frac{1}{4}T} \tag{16}$$

Where:

T: is the period of the sound

We use the same method to estimate the value of $\frac{\partial^2 u}{\partial t^2}$

$$\frac{\partial^2 u}{\partial t^2} \approx \frac{\frac{\partial u}{\partial t}}{\frac{1}{4}T} \approx \frac{u}{\left(\frac{1}{4}T\right)^2} \tag{17}$$

We acknowledge that is not an accurate way of calculating the values of $\frac{\partial u}{\partial t}$ and $\frac{\partial^2 u}{\partial t^2}$ as we do not actually know the waveform of u(t), but it is accurate enough for an order of magnitude estimate. The period of audio in our experiments varies between 1/50 and 1/1000, so we will use $T \approx 10^{-2}$ in our estimates. Using this estimate of period and the estimate of u from Equation 15, we calculate $\frac{\partial u}{\partial t}$ and $\frac{\partial^2 u}{\partial t^2}$:

$$\frac{\partial u}{\partial t} \approx 10^0 m s^{-2} \tag{18}$$

$$\frac{\partial^2 u}{\partial t^2} \approx 10^2 m s^{-3} \tag{19}$$

We also need an estimate of of $\frac{\partial p}{\partial r}$, so we rearrange Equations 11,12,13 to solve for P_{rms} and use the method shown in figure 17 to calculate $\frac{\partial p}{\partial r}$:

$$P_{rms} = \sqrt{I_0 10^{\left(\frac{A}{10}\right)} \rho c} \tag{20}$$

$$\frac{\partial p}{\partial r} \approx \frac{P_{rms}}{\frac{1}{4}cT} \tag{21}$$

$$\frac{\partial p}{\partial r} \approx 10^0 kgm^{-2}s^{-2} \tag{22}$$

Lastly, we just need estimates for all the coefficients in Equation 10. For these, we use the following literature values:

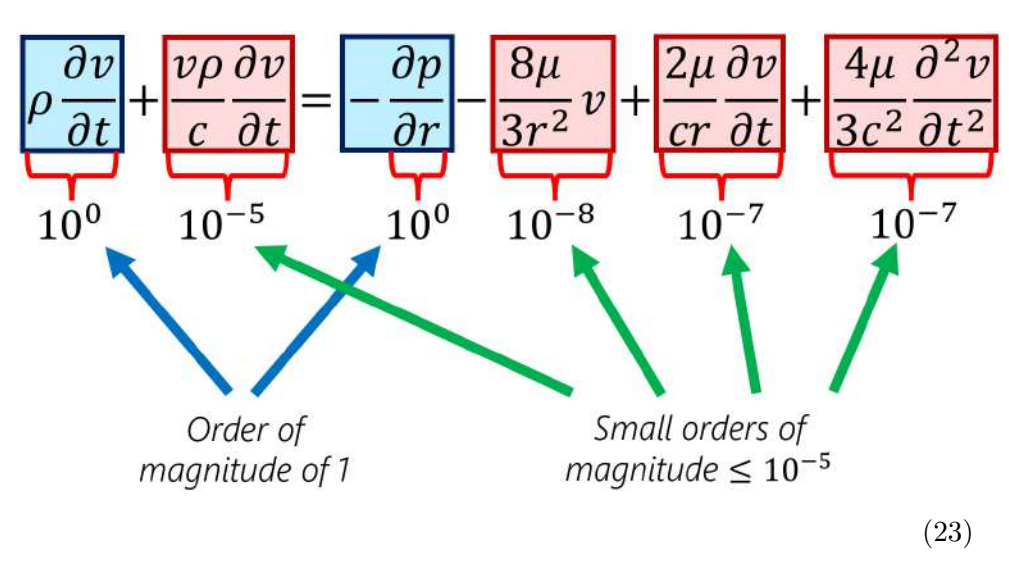
$$\mu \approx 10^{-5} kgm^{-1}s^{-1}$$

$$r \approx 10^0 m$$

$$\rho \approx 10^0 kgm^{-3}$$

$$c \approx 10^2 ms^{-1}$$

Here, μ is the dynamic viscosity of air, r is the distance between the point source and the microphone, ρ is the density of air and c is the speed of sound in air. With that, we have estimates for every term in Equation 10:



By looking at the order of magnitudes of each term, we can see that only the first and terms are significant, as they have orders of magnitude of 1. The rest of the terms all have orders of magnitude smaller than 10^{-5} , so we can safely neglect them. After removing them, we are left with the following equation

$$\rho \frac{\partial v}{\partial t} = -\frac{\partial p}{\partial r} \tag{24}$$

2.2.3 Directional Microphone

We then proceed to consider the pressure gradient microphone. We assert that the microphone measures the negative spatial rate of change of pressure in the direction it's pointed at, which would be the negative dot product of the normal vector and the pressure gradient vector:

$$SPL \propto -\hat{n} \cdot \nabla p$$
 (25)

Where:

SPL: is the Sound Pressure Level

Given we assume spherical symmetry, we can get rid of the dependence on the position of the microphone from Equation 25:

$$\hat{n} \cdot \nabla p = \frac{\partial p}{\partial r} \left(\hat{n} \cdot \hat{r} \right) \tag{26}$$

Lastly, we combine Equation 24 and 26 to get an expression for the Sound Pressure Level generated by a Seebeck Siren:

$$SPL \propto \frac{\partial v}{\partial t}$$
 (27)

2.2.4 Volume flow rate through a Seebeck Siren

Now that we have a function of the Sound Pressure Level in terms of the partial derivative of the velocity of air with respect to time, we will solve for the volume flow rate of air through a Seebeck Siren. According to (Hussein et al., 1994), the velocity profile of a fully developed air flow exiting a nozzle can be approximated with a Gaussian function[5]:

$$f(x) = ae^{-\frac{x-b^2}{2c^2}} (28)$$

Where:

a: is the height of the peak

b: is the position of the center of the peak

c: is the standard deviation

Thus, we model the velocity profile of our nozzle as a 2D Gaussian function at the center of the nozzle. We do so by integrating over the nearest hole to solve for our volume flow rate, using l and f as integration constants:

$$Q(t) = \int_{-r_1}^{r_1} \int_{-\sqrt{r_1^2 - f^2}}^{\sqrt{r_1^2 - f^2}} e^{-\frac{t^2 + \left(2r\sin(\frac{\pi tf}{q}) - f\right)^2}{2c^2}} dldf$$
 (29)

Where:

Q: is the volume flow rate through the disk

f: is the frequency of rotation

q: is the number of holes

r: is the distance from the hole to the center of the disk

 r_1 : is the radius of the hole in the disk

Plotting this, we may observe the flow rate through the disks as a function of time:

Since we assume our siren is a point source, the flow rate through the disk is proportional to the velocity of air at the microphone:

$$Q(t) \propto v(t) \tag{30}$$

From this, it becomes obvious that

$$\frac{\partial v}{\partial t} \propto \frac{\mathrm{d}Q}{\mathrm{d}t}$$
 (31)

Using the expression of the Sound Pressure Level from Equation 27 and the flow rate from Equation 29, we can formulate an expression of the Sound Pressure Level in terms of the flowrate:

$$SPL \propto \frac{\mathrm{d}Q}{\mathrm{d}t}$$
 (32)

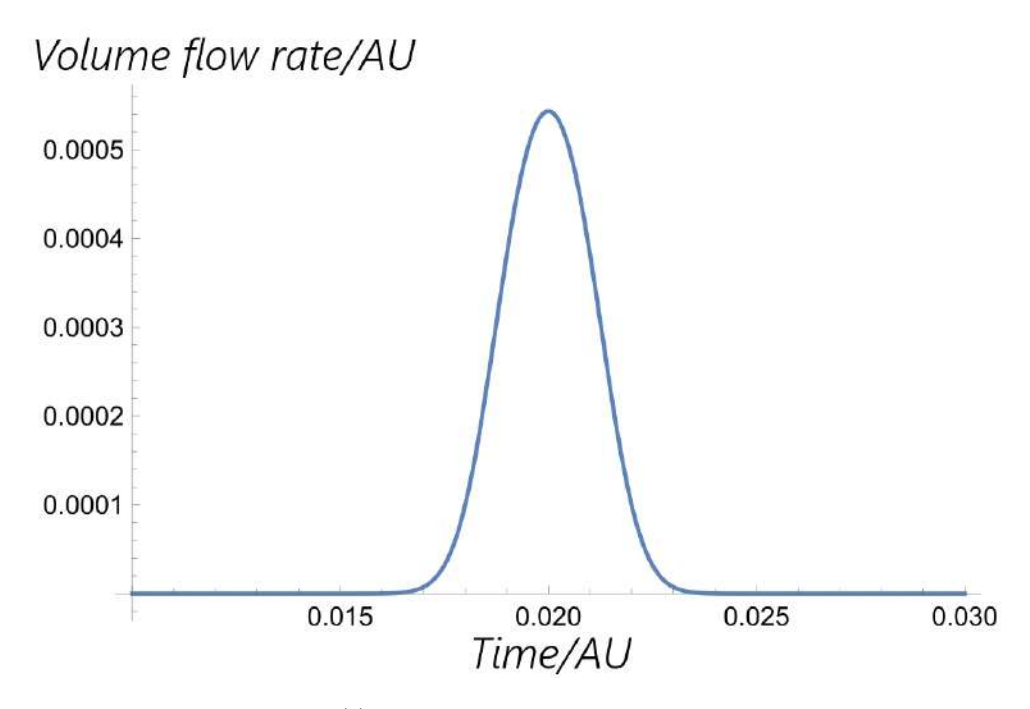


Figure 3: Q(t) plotted with an arbitrary time scale

We can plot this in Figure 4 to get our theoretical prediction of the waveform generated by the Siren. We note that the computation of this waveform averages less than half a second on a consumer laptop, and fulfills our original goal of creating a low computational intensity model. Computing a similar, more complete model using the $k-\omega$ turbulence model on the same device requires 21 hours and 47 minutes, taking almost a whole day to do, achieving more than a 99.999% reduction in computation time.

2.3 Experimental Verification

2.3.1 Experimental Setup

For our experimental setup, we spun a 3D-printed disk using a brushless motor and recorded the sound produced using a shotgun microphone. The microphone we used is the RØDE NTG2, as it had a very flat frequency

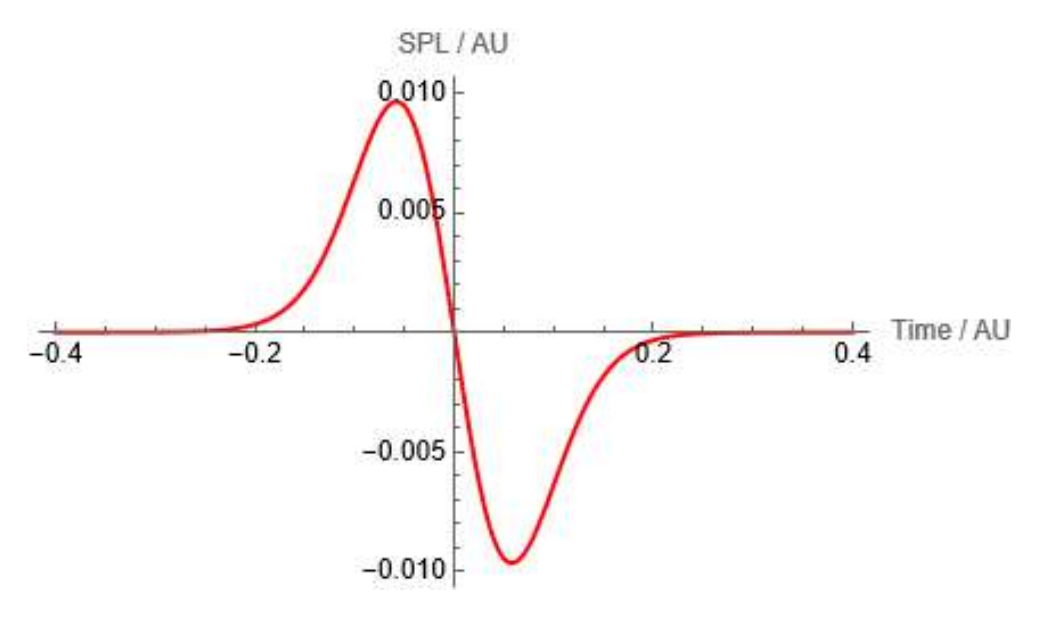


Figure 4: Theoretical waveform of the audio produced by a Seebeck Siren

response curve, ensuring that the data collected accurately represents the actual sound generated in this frequency range. For reference, the frequency response curve can be seen in Appendix B.

In the experimental setup, the microphone is placed about 10cm away from the disk at an angle such that it is not directly in the air stream. The disk is spun with a brushless motor instead of the more common brushed motor as brushless motors produce less noise.

2.3.2 Data Processing Techniques

Experimentally, we notice that the collected data is quite noisy, which you may notice in Figure 6

To process the data, we take the Fourier transform of the audio and remove any non-harmonic components. The before and afters can be seen in Figure 7.

The reason we do so is because non-harmonics are either noise or hys-

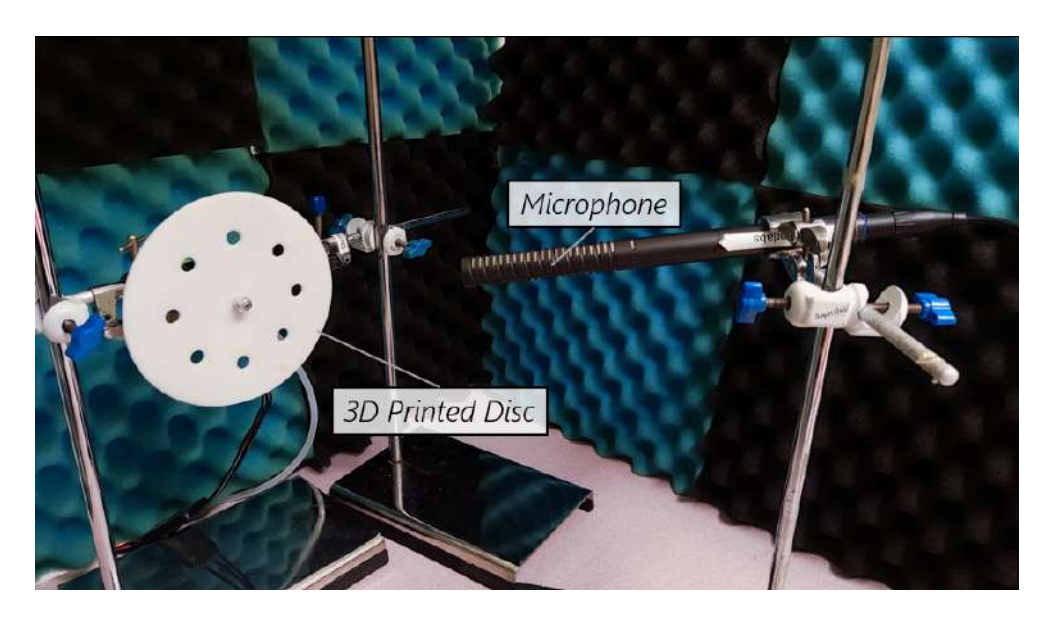


Figure 5: Picture of the experimental setup

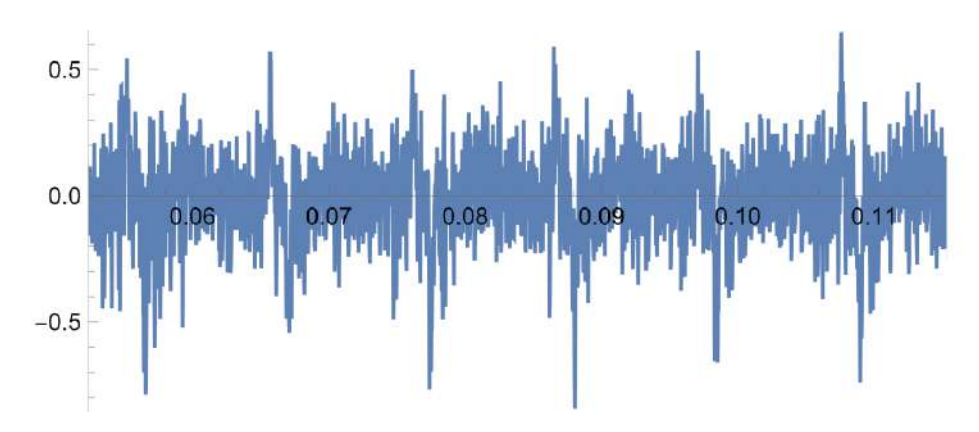


Figure 6: Experimental plot of Sound Pressure Level over time

teresis. If the non-harmonics are due to noise, such as turbulent vortices from the air jet or background noise, then removing it would give us a better representation of the sound generated by the siren. It is also possible that these non-harmonics are a form of hysteresis, where the waveform is affected by the shape of the previous waveform, but accounting for it would be much more computationally intensive and would not provide much physical

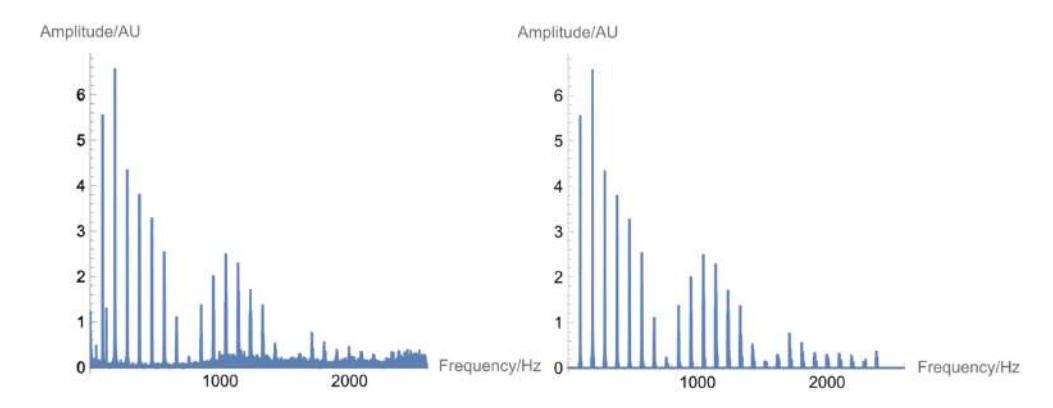


Figure 7: Figure 7 (left) shows the FFT before processing, and Figure 7 (right) shows the FFT after processing

insight. Thus, we get rid of it and remove the non-periodic harmonics, acquiring a more accurate representation of the periodic behavior of the siren. Then, we take an inverse Fourier transform to convert the clean Fourier transform back into a waveform:

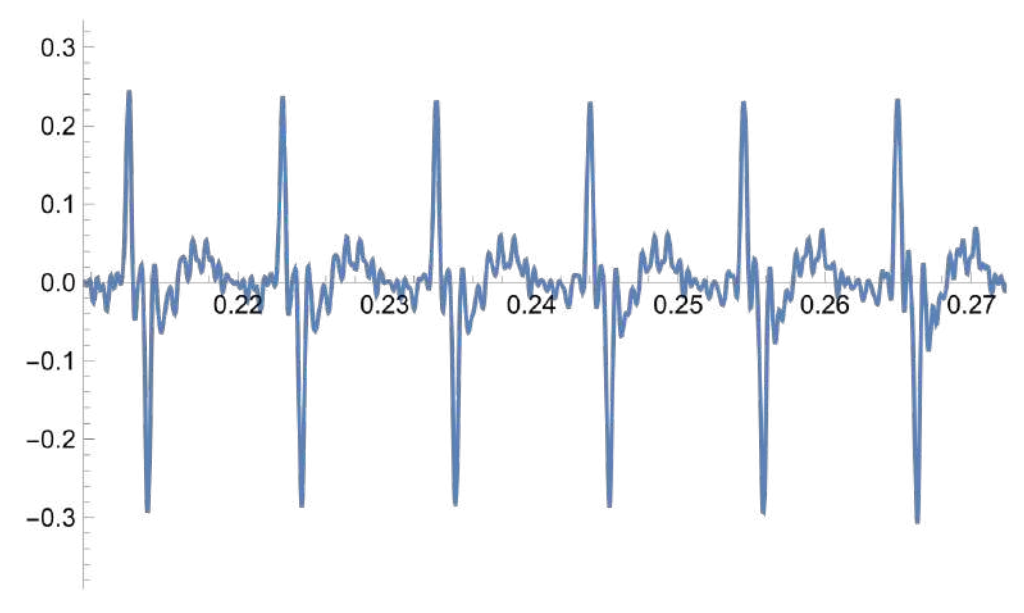


Figure 8: Experimental audio waveform after processing the non-harmonic components $\,$

2.3.3 Experiment Theory Comparison

To solve for the flow rate, we require the value of the standard deviation of our velocity profile, which is a constant we use in our Gaussian in Equation 29 that describes the characteristics of the airflow. To calculate this, we fitted the value to one experiment and used the same value for all our experiments. For all the following graphs, we used a standard deviation of c=0.0025. Using this value, we compare the experimental data with the theory for a disk with 4 holes that are of 1cm radius each:

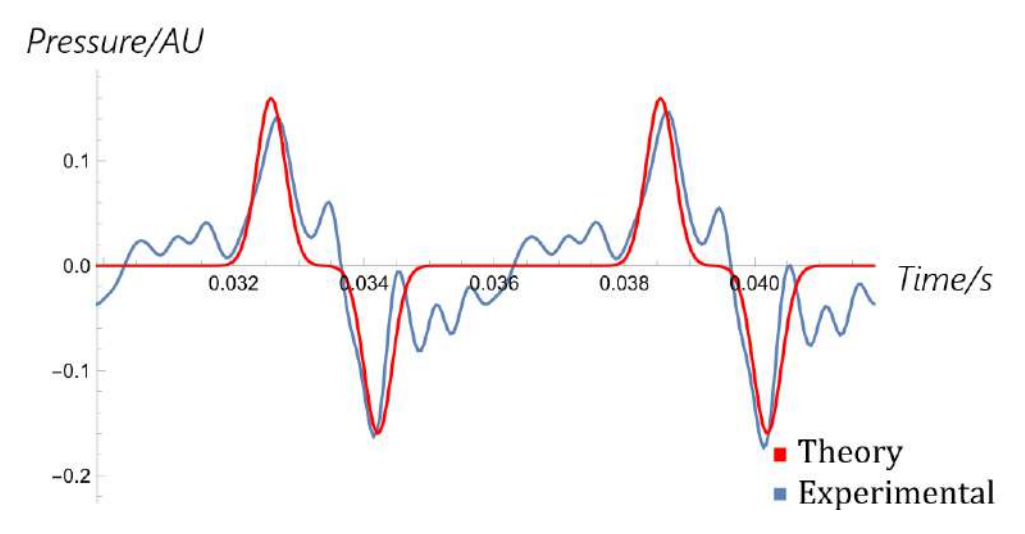


Figure 9: Experiment theory comparison for a disk with 4 holes that are of 1cm radius. The Fourier transform of this data is included in Appendix C

The under-prediction right after the peak and over-prediction after the trough could be due to the flexing of the disk, as it is 3D printed out of PLA and is only 0.2cm. It could also be due to higher-order effects that were neglected in the theory for the sake of simplification. In Figure 9, you can see that the peaks appear wider than in Figure 10. This makes sense as having more holes means that more time is spent with the nozzle near the disk, hence resulting in a wider peak. Comparing Figure 11 and 9, we can see

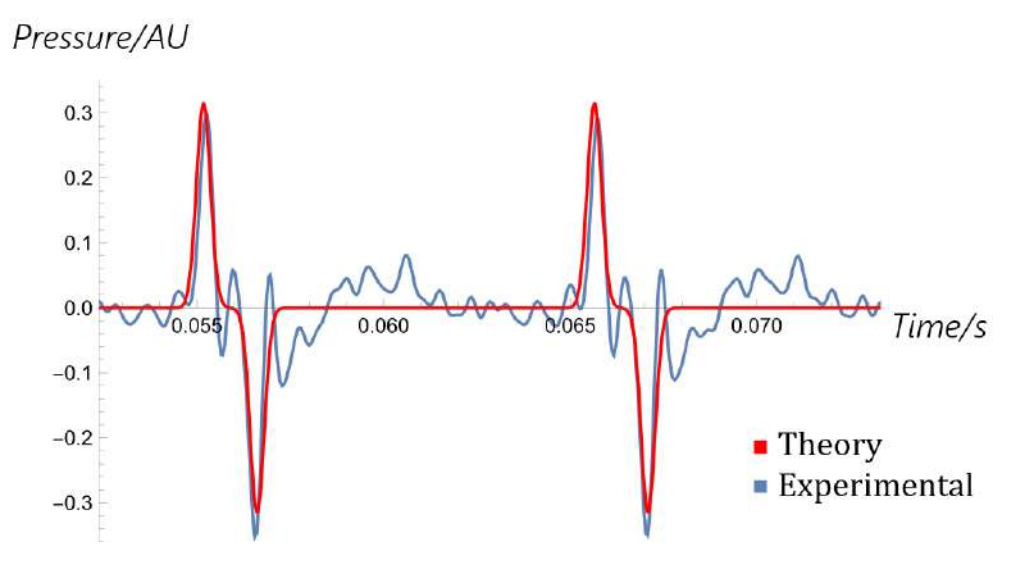


Figure 10: Experiment theory comparison for a disk with 2 holes that are of 1cm radius. The Fourier transform of this data is included in Appendix D $\,$

Pressure/AU

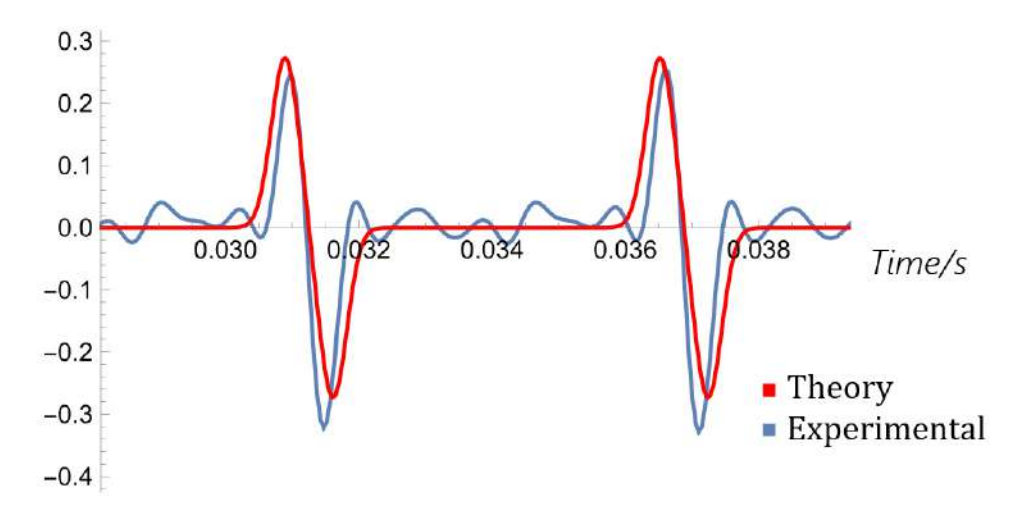


Figure 11: Experiment theory comparison for a disk with 4 holes that are of 0.5cm radius. The Fourier transform of this data is included in Appendix ${\bf E}$

that decreasing the hole size decreases the width of the peak slightly. The plateau between the peak and the trough also disappears. This is because when the hole radius is large and the nozzle is centered at the hole, any movement of the nozzle results in a small change of flow rate, causing a plateau as the waveform is the rate of change of flow rate. On the other hand, when the hole radius is small, changing the position of the nozzle slightly results in a large change in flow rate, causing no plateau between the peak and the trough, which is a pattern we can see in both the theory and experimental graphs.

2.3.4 Observed Asymmetry

In all of our data, we observed that there was an asymmetry in the audio, where the troughs of the experimental data were almost always of a greater height than the peaks. This can be observed in Figure 8, 9, 10 and 11. We theorize that this is because of the skin drag on the surface of the disk. In Figure 12, you can see the velocity profile of the air jet (blue lines) before and after the disk has begun spinning. This is because of skin drag, as the moving surface of the disk pulls the air along with it, thus causing the air to move faster in the direction of spin. As the air has a lower velocity on the approaching side of the disk, the pressure is higher, thus resulting in a higher flow rate:

Plotting the graph of flowrate, we can thus see that the change in flow rate on approach is smaller than the change in pressure on moving away:

The Sound Pressure Level is proportional to the change in flow rate, so since the change in flow rate as the hole approaches is less than the change in flow rate as the hole moves away, asymmetry occurs in the Sound Pressure Level, which can be seen in Figure 15. To test our hypothesis, we provide constant airflow to a disk while increasing the speed of the rotation.

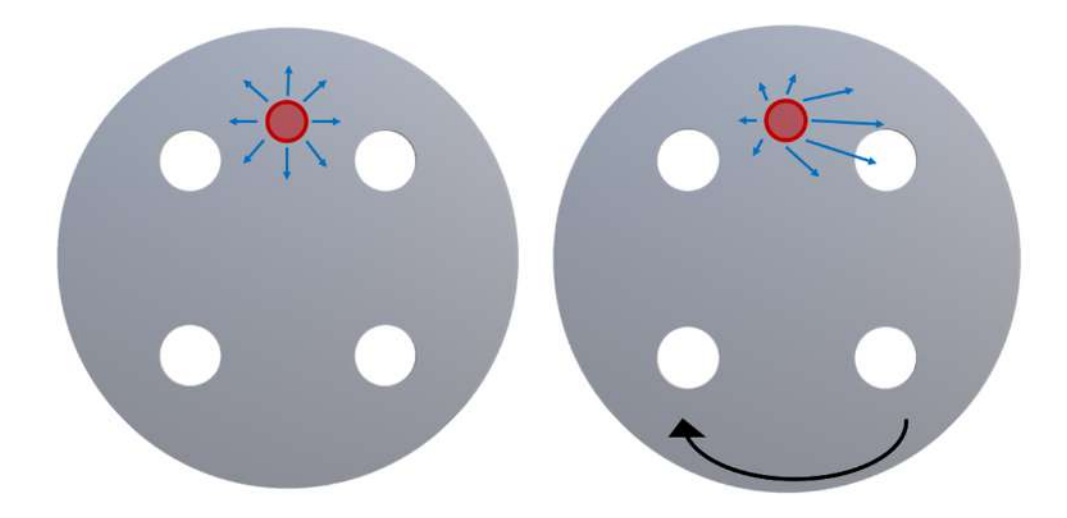


Figure 12: Figure 12 (left) shows the uniform velocity profile when the disk is not spinning. Figure 12 (right) shows the velocity profile elongated in the direction of spin.

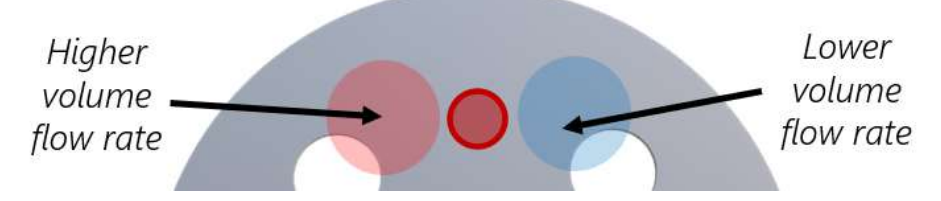


Figure 13: The volume flow rate on approach is greater than the flow rate as the hole moves away

According to our hypothesis, as the disk spins faster, the asymmetry would be larger as the higher angular velocity results in more skin drag.

In Figure 16, we observe that the asymmetry does indeed worsen when the disk is spun faster, supporting our theory of skin drag being the cause of asymmetry.

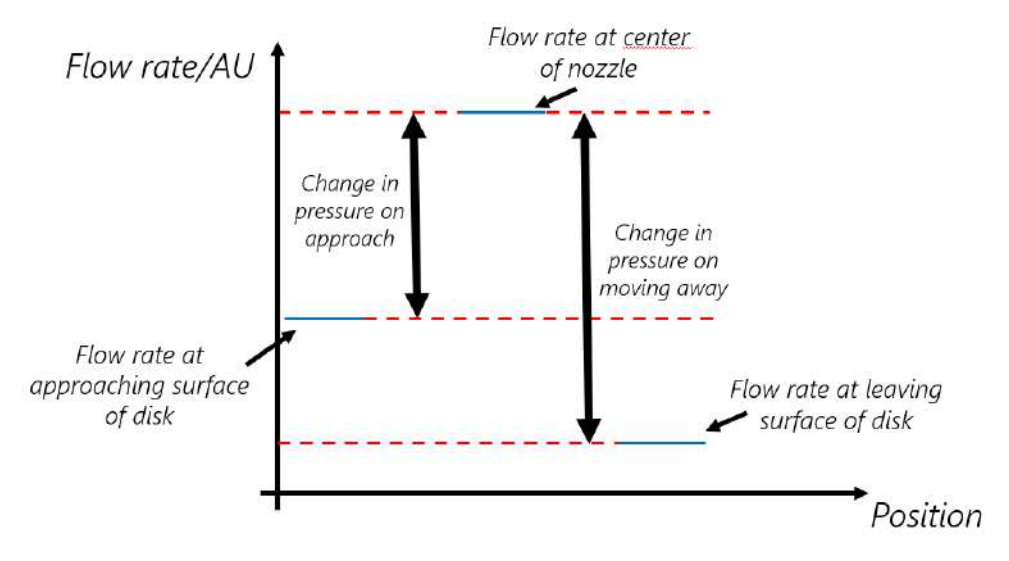


Figure 14: Plot of flow rate as a function of the angular position of the disk. This graph is not to scale and is only for qualitative understanding 99.999

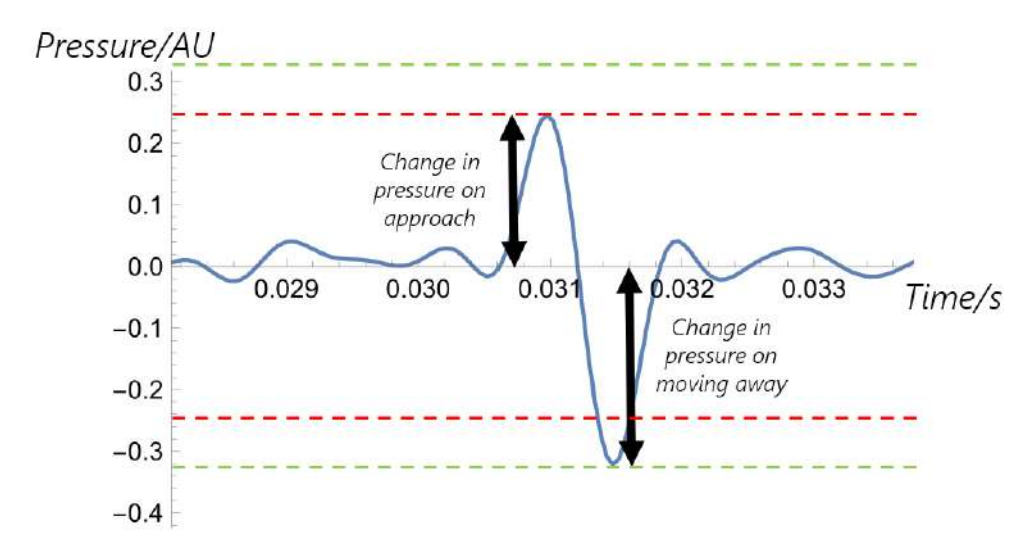


Figure 15: Experimentally observed asymmetry

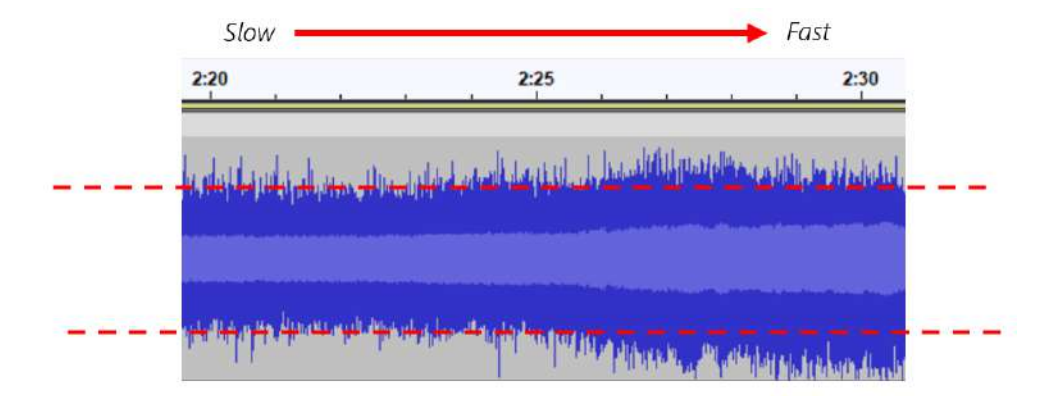


Figure 16: Experimental audio of a disk increasing in angular velocity. The dotted lines represent the peak and troughs of data without asymmetry

3 Conclusion

We have presented a simplified but mostly accurate model for solving for the sound generated by a Seebeck Siren. Overall, we observe that the general trend of the theory and experiment matches quite well. Despite the many simplifications made to the theory, the theory still has predictive power for the waveform. The model also provides physical insight and understanding into the phenomenon and clearly shows the relation between the airflow and the sound produced. The deviations were explained, and the reason for asymmetry has been experimentally verified.

It should be noted that this model is only applicable to similar phenomena, as some of the simplifications in Equation 23 may not be valid in different cases. However, similar methods may be used to simplify the phenomenon, should the exact simplifications in this model not be applicable.

4 Future Work

We wish to investigate disks of different shapes to verify the applicability of the assumptions made in this theory. It should require little effort to research as the theory should remain the same. Using stiffer disks may also reduce some of our experimental errors and tell us if the misfits are purely experimental.

A Derivation of radially symmetric Navier-Stokes in spherical coordinates

To derive the radially symmetric compressible Navier-Stokes, we begin with the compressible Navier-Stokes in cartesian coordinates:

$$\rho \left(\frac{\partial \mathbf{u}}{\partial t} + (\mathbf{u} \cdot \nabla) \mathbf{u} \right) = -\nabla p + \mu \nabla^2 \mathbf{u} + \frac{1}{3} \mu \nabla (\nabla \cdot \mathbf{u})$$
 (33)

First, we expand $\frac{\partial \mathbf{u}}{\partial t}$ into spherical coordinates:

$$\frac{\partial u_r}{\partial t}\hat{\mathbf{r}} + \frac{\partial u_\theta}{\partial t}\hat{\boldsymbol{\theta}} + \frac{\partial u_\varphi}{\partial t}\hat{\boldsymbol{\varphi}}$$
(34)

Since we assume radial symmetry, $\hat{\theta}$ and $\hat{\varphi}$ are both 0 as the velocity field will only point away from the origin, leaving \hat{r} as the only non-zero term. This means that we can remove the second and third term, leaving us with:

$$\frac{\partial u_r}{\partial t}\hat{\mathbf{r}} \tag{35}$$

Now we can deal with the second term, which is $(\mathbf{u} \cdot \nabla)\mathbf{u}$. Expanding it into spherical coordinates, we get a very big and intimidating-looking equation:

$$\left(u_{r}\frac{\partial u_{r}}{\partial r} + \frac{u_{\theta}}{r}\frac{\partial u_{r}}{\partial \theta} + \frac{u_{\varphi}}{r\sin\theta}\frac{\partial u_{r}}{\partial \varphi} - \frac{u_{\theta}^{2} + u_{\varphi}^{2}}{r}\right)\hat{\mathbf{r}}$$

$$+ \left(u_{r}\frac{\partial u_{\theta}}{\partial r} + \frac{u_{\theta}}{r}\frac{\partial u_{\theta}}{\partial \theta} + \frac{u_{\varphi}}{r\sin\theta}\frac{\partial u_{\theta}}{\partial \varphi} + \frac{u_{\theta}u_{r}}{r} - \frac{u_{\varphi}^{2}\cot\theta}{r}\right)\hat{\boldsymbol{\theta}} \qquad (36)$$

$$+ \left(u_{r}\frac{\partial u_{\varphi}}{\partial r} + \frac{u_{\theta}}{r}\frac{\partial u_{\varphi}}{\partial \theta} + \frac{u_{\varphi}}{r\sin\theta}\frac{\partial u_{\varphi}}{\partial \varphi} + \frac{u_{\varphi}u_{r}}{r} + \frac{u_{\varphi}u_{\theta}\cot\theta}{r}\right)\hat{\boldsymbol{\varphi}}$$

However, upon inspection, we see that the second and third term are multiplied by $\hat{\theta}$ and $\hat{\varphi}$ respectively, which are both 0. We can also remove every single term that has $\partial \theta$ or $\partial \varphi$, as well as u_{θ} and u_{φ} . This leaves us with just this term:

$$\left(u_r \frac{\partial u_r}{\partial r}\right) \hat{r} \tag{37}$$

Onto the third term, we expand $-\nabla p$ into spherical coordinates:

$$-\left(\frac{\partial p}{\partial r}\hat{\mathbf{r}} + \frac{1}{r}\frac{\partial p}{\partial \theta}\hat{\boldsymbol{\theta}} + \frac{1}{r\sin\theta}\frac{\partial p}{\partial \varphi}\hat{\boldsymbol{\varphi}}\right)$$
(38)

Because of the $\partial\theta$ or $\partial\varphi$, the second and third terms are both zero, leaving us with:

$$-\frac{\partial p}{\partial r}\hat{\mathbf{r}}\tag{39}$$

Next, we have the Vector Laplacian, $\mu \nabla^2 \mathbf{u}$. We expand it into spherical

coordinates to get:

$$\left(\nabla^{2}u_{r} - \frac{2u_{r}}{r^{2}} - \frac{2}{r^{2}\sin\theta} \frac{\partial\left(u_{\theta}\sin\theta\right)}{\partial\theta} - \frac{2}{r^{2}\sin\theta} \frac{\partial u_{\varphi}}{\partial\varphi}\right)\hat{\mathbf{r}}
+ \left(\nabla^{2}u_{\theta} - \frac{u_{\theta}}{r^{2}\sin^{2}\theta} + \frac{2}{r^{2}} \frac{\partial u_{r}}{\partial\theta} - \frac{2\cos\theta}{r^{2}\sin^{2}\theta} \frac{\partial u_{\varphi}}{\partial\varphi}\right)\hat{\boldsymbol{\theta}}
+ \left(\nabla^{2}u_{\varphi} - \frac{u_{\varphi}}{r^{2}\sin^{2}\theta} + \frac{2}{r^{2}\sin\theta} \frac{\partial u_{r}}{\partial\varphi} + \frac{2\cos\theta}{r^{2}\sin^{2}\theta} \frac{\partial u_{\theta}}{\partial\varphi}\right)\hat{\boldsymbol{\varphi}}$$
(40)

The $\hat{\theta}$ and $\hat{\varphi}$ terms disappear since there is radial symmetry, leaving us with:

$$\left(\nabla^2 u_r - \frac{2u_r}{r^2} - \frac{2}{r^2 \sin \theta} \frac{\partial \left(u_\theta \sin \theta\right)}{\partial \theta} - \frac{2}{r^2 \sin \theta} \frac{\partial u_\varphi}{\partial \varphi}\right) \hat{\mathbf{r}} \tag{41}$$

Any term with $\partial\theta$ or $\partial\varphi$ also disappears, as their gradients are zero, reducing the equation further to:

$$\left(\nabla^2 u_r - \frac{2u_r}{r^2}\right)\hat{\mathbf{r}}\tag{42}$$

Now we expand the Laplace operator, which is the $\mu \nabla^2 u_r$ term:

$$\mu \left(\frac{1}{r^2} \frac{\partial}{\partial r} \left(r^2 \frac{\partial u_r}{\partial r} \right) + \frac{1}{r^2 \sin \theta} \frac{\partial}{\partial \theta} \left(\sin \theta \frac{\partial u_r}{\partial \theta} \right) + \frac{1}{r^2 \sin^2 \theta} \frac{\partial^2 u_r}{\partial \varphi^2} \right) \tag{43}$$

Removing the $\partial\theta$ and $\partial\varphi$ terms and substituting it back into Equation 42, we get:

$$\mu \left(\frac{1}{r^2} \frac{\partial}{\partial r} \left(r^2 \frac{\partial u_r}{\partial r} \right) - \frac{2u_r}{r^2} \right) \hat{\mathbf{r}}$$
 (44)

Completing the differentiation, the result is:

$$\mu \left(\frac{2}{r} \frac{\partial u_r}{\partial r} + \frac{\partial^2 u_r}{\partial r^2} - \frac{2u_r}{r^2} \right) \hat{\mathbf{r}}$$
 (45)

Finally, we move on to $\frac{1}{3}\mu\nabla(\nabla\cdot\mathbf{u})$. Expanding the divergence of u, which

is $\nabla \cdot \mathbf{u}$, we get:

$$\frac{1}{r^2} \frac{\partial (r^2 u_r)}{\partial r} + \frac{1}{r \sin \theta} \frac{\partial}{\partial \theta} (u_\theta \sin \theta) + \frac{1}{r \sin \theta} \frac{\partial u_\varphi}{\partial \varphi}$$
(46)

We remove the $\partial\theta$ and $\partial\varphi$ terms and differentiate it to get:

$$\frac{1}{3}\mu\nabla(\frac{2u_r}{r} + \frac{\partial u_r}{\partial r})\tag{47}$$

Expanding ∇f gives us the following:

$$\frac{\partial f}{\partial r}\hat{\mathbf{r}} + \frac{1}{r}\frac{\partial f}{\partial \theta}\hat{\boldsymbol{\theta}} + \frac{1}{r\sin\theta}\frac{\partial f}{\partial \varphi}\hat{\boldsymbol{\varphi}} \tag{48}$$

Which reduces to:

$$\frac{\partial f}{\partial r}\hat{\mathbf{r}}\tag{49}$$

We then use the identity in Equation 49 to expand Equation 47:

$$\left(\frac{\partial^2 u_r}{\partial r^2} - \frac{2u_r}{r^2}\right)\hat{\mathbf{r}}\tag{50}$$

Now, we have all the terms in terms of spherical coordinates. Combining them, we get:

$$\rho \left(\frac{\partial u}{\partial t} + u \frac{\partial u}{\partial r} \right) \hat{r} = -\frac{\partial p}{\partial r} \hat{r}$$

$$+ \left(\frac{2}{r} \frac{\partial u}{\partial r} + \frac{\partial^2 u}{\partial r^2} - \frac{2u}{r^2} \right) \hat{r} + \left(\frac{\partial^2 u}{\partial r^2} - \frac{2u}{r} \right) \hat{r}$$

$$(51)$$

Simplifying the equation, we end up with our final equation of the radially

symmetric compressible Navier-Stokes in terms of spherical coordinates:

$$\rho \left(\frac{\partial u}{\partial t} + u \frac{\partial u}{\partial r} \right) = -\frac{\partial p}{\partial r} - \frac{8\mu}{3r^2} u + \frac{2\mu}{r} \frac{\partial u}{\partial r} + \frac{4\mu}{3} \frac{\partial^2 u}{\partial r^2}$$
 (52)

B Frequency response of microphone

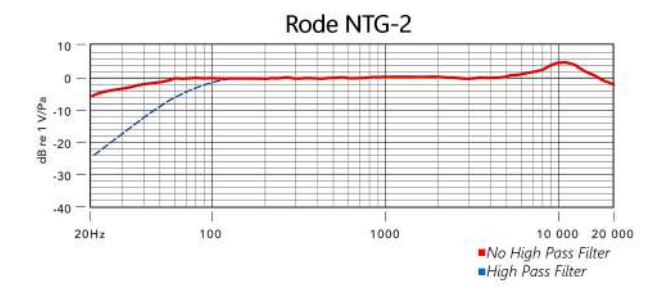
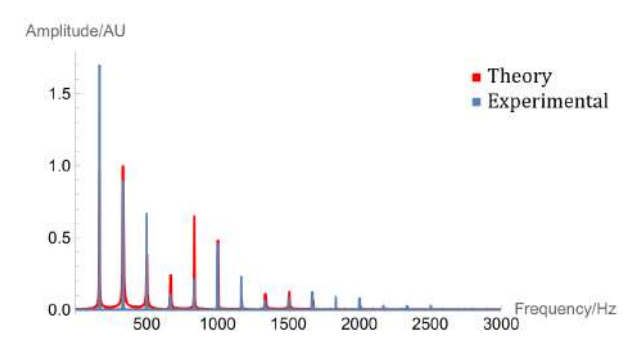


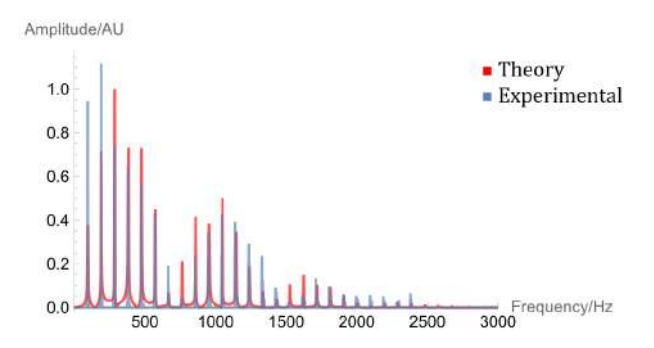
Figure 17: Experimental audio waveform after processing the non-harmonic components

C Fourier Transform, 4 holes of 1cm radius



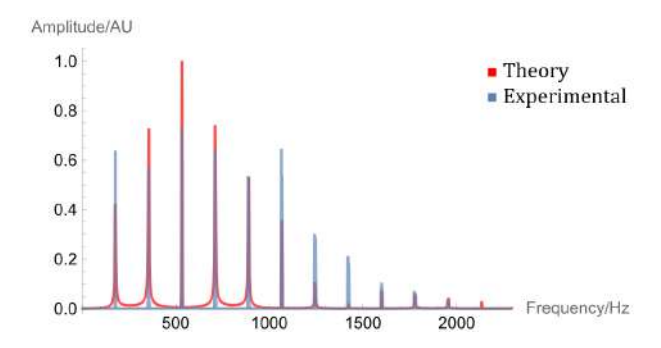
Fourier Transform for a disk of 4 holes of 1cm radius each

D Fourier Transform, 2 holes of 1cm radius



Fourier Transform for a disk of 2 holes of 1cm radius each

E Fourier Transform, 4 holes of 0.5cm radius



Fourier Transform for a disk of 4 holes of 0.5cm radius each

References

- [1] Del in cylindrical and spherical coordinates. https://en.wikipedia.org/wiki/Del_in_cylindrical_and_spherical_coordinates [Accessed: (2023-12-15)].
- [2] CH Allen and I Rudnick. A powerful high frequency siren. The Journal of the Acoustical Society of America, 19(5):857–865, 1947.
- [3] Edwin Garrigues Boring and SS Stevens. The nature of tonal brightness. *Proceedings* of the National Academy of Sciences, 22(8):514–521, 1936.
- [4] Regina Collecchia, Dan Somen, and Kevin McElroy. The siren organ. In *NIME*, pages 391–394, 2014.
- [5] Hussein J Hussein, Steven P Capp, and William K George. Velocity measurements in a high-reynolds-number, momentum-conserving, axisymmetric, turbulent jet. *Journal* of Fluid Mechanics, 258:31–75, 1994.
- [6] Brian Edward Launder and Bahrat I Sharma. Application of the energy-dissipation model of turbulence to the calculation of flow near a spinning disc. Letters in heat and mass transfer, 1(2):131–137, 1974.
- [7] Max F Meyer. New auditory phenomena from siren experiments. *The American Journal of Psychology*, 77(3):414–421, 1964.
- [8] Edward Arthur Milne and Ralph Howard Fowler. Siren harmonics and a pure tone siren. Proceedings of the Royal Society of London. Series A, Containing Papers of a Mathematical and Physical Character, 98(694):414–427, 1921.
- [9] Roger Hinrichs Paul Peter Urone. Physics. OpenStax, Houston, Texas, 2020.

【評語】160034

Simplified Approach for Real-World Applications.

This project aims to understand the Seebeck sirens by proposing a simplified equation to approximate the Navier-Stokes equations by neglecting the non-linear terms. Interestingly an effect of air drag is proposed to describe the difference in experimental and theoretical result. It's a solid work with nice theoretical analysis. However the report could provide a more in-depth discussion about the effect of neglected non-linear terms.